Hybridization of Rydberg Electron Orbitals by Molecule Formation

A. Gaj,* A. T. Krupp, P. Ilzhöfer, R. Löw, S. Hofferberth, and T. Pfau†
5. Physikalisches Institut and Center for Integrated Quantum Science and Technology, Universität Stuttgart, Pfaffenwaldring 57, 70569 Stuttgart, Germany
(Received 16 March 2015; published 8 July 2015)

The formation of ultralong-range Rydberg molecules is a result of the attractive interaction between a Rydberg electron and a polarizable ground-state atom in an ultracold gas. In the nondegenerate case, the backaction of the polarizable atom on the electronic orbital is minimal. Here we demonstrate how controlled degeneracy of the respective electronic orbitals maximizes this backaction and leads to stronger binding energies and lower symmetry of the bound dimers. Consequently, the Rydberg orbitals hybridize due to the molecular bond.

DOI: 10.1103/PhysRevLett.115.023001 PACS numbers: 32.80.Ee, 31.10.+z, 33.15.Dj, 33.20.-t

The geometrical structure of molecules determines their physical and chemical properties. The shape of an individual molecular bond can be explained by the concept of hybridization. The mixing of nearly degenerate atomic orbitals leads to a new hybrid orbital, which allows one to analyze structures of many basic molecules like carbon dioxide, ammonia, or water. One of the first molecules described this way was methane [1]. In CH_4, the carbon electrons, initially in an s or p configuration, are rearranged into four hybrid orbitals sp^3 while creating the molecular bond. The new hybrid orbital contains 25% s character and 75% p character.

Here, we present the hybridization of a Rydberg electron orbital induced by the formation of an ultralong-range Rydberg molecule. Here, Rydberg molecules consist of a single Rydberg atom bound to one or more ground-state atoms. The bond in this type of molecule originates from the elastic scattering between the slow Rydberg electron and a ground-state atom. Diatomic Rydberg molecules have been observed for S-states [2,3], D-states [4,5], and P-states [6,7] in gases of Rb or Cs. Polyatomic Rydberg molecules have been recently photoassociated from a gas of Rb [8]. The presence of the neutral perturber inside the Rydberg electron orbital can cause admixing with a nearly degenerate hydrogenic manifold and energetically close by l-states at the location of the ground-state atom [9]. As a result, these so-called trilobite molecules can possess a giant permanent electric dipole moment. For Cs, which has an almost integer quantum defect for the S-state, this admixture can amount to 90% and lead to a permanent dipole moment of kilodebye, which was shown in Ref. [10] for principal quantum numbers $n = 37, 39, 40$. In Rb, the hydrogenic manifold is energetically much further away. Therefore, the hydrogenic admixture was less then 1% and the observed permanent dipole moments were on the order of 1D for $n = 35, 43$ [11]. In this paper, unlike in the experiments with trilobite states, we do not mix many states with different principal and angular quantum numbers. We demonstrate the perturber-induced formation of a new hybrid orbital, which is a linear combination of only two m_j-states with known orbital shapes. This differs from typical hybridization of orbitals with different angular momentum [1]. Our experiment is a textbooklike example of tunable hybridization in the field of Rydberg molecules. The ratio of the contributing states can be precisely controlled by an applied electric field. This allows for tuning the contribution of one m_j-state to the hybrid orbital from 0 to 100% over the crossing of the two m_j-states.

In the absence of an external field, the magnetic substates of the Rydberg energy levels are degenerate. This degeneracy can be lifted by applying a magnetic field B. The initially degenerate states are then split into $2j + 1$ different Zeeman levels labeled by the projection of the total angular momentum on the quantization axis m_j. Individual m_j-states can be brought back to degeneracy by applying an additional electric field $\mathcal{E}$ aligned parallel to the B field. In Fig. 1, calculated Stark maps in the vicinity of the $42D$ state in an external magnetic field of $B = 13.55$ G are shown. The eigenenergies are obtained by diagonalizing the full Hamiltonian consisting of an unperturbed atomic Hamiltonian and two terms accounting for the interaction with the magnetic and electric fields. The splitting between states of different quantum numbers l, with $l \leq 3$ is caused by their quantum defects [12,13]. These states exhibit a quadratic Stark effect, as can be seen for the $42D_{5/2}$ state, which splits into six m_j levels, shown in the magnification of Fig. 1. States of the manifold with $l > 3$ show a linear Stark effect, which results in a fanlike Stark structure. The magnitude of the corresponding shifts depends on the absolute value of m_j. Since the electric and magnetic dipole operators do not couple states of $\Delta m_j \neq 0$ for $\mathcal{E} \| B$, the $m_j = 5/2$ and $m_j = 1/2$ states become degenerate at $\mathcal{E} = 1.135$ V/cm exhibiting real crossing. The absence of coupling between the atomic states provides a clean two-level system, suitable for the investigation of

 © 2015 American Physical Society

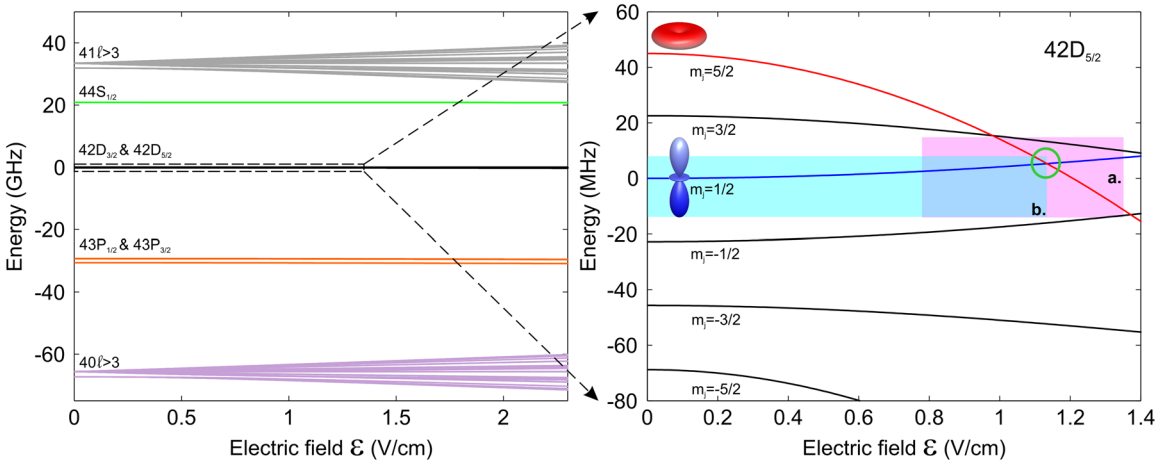

FIG. 1 (color online). Calculated Stark map of the atomic states in the vicinity of the $42D$ state for ^{87}Rb. The electric field is aligned parallel to the magnetic field $B = 13.55$ G. All energies are plotted relative to the energy of the $42D_{5/2}, m_j = 1/2$ atomic state at $\mathcal{E} = 0$. The states are labeled with quantum numbers of the states they adiabatically unite with at $\mathcal{E} = 0$. In the magnification, the Zeeman splitting of the $42D_{5/2}$ manifold is visible. The green circle marks the investigated atomic crossing of the $m_j = 1/2$ (blue) and $m_j = 5/2$ (red) energy levels. The part of the spherical harmonics that is relevant for the molecule formation at $\mathcal{E} = 0$ is depicted close to the corresponding levels. The shaded areas (a) (magenta) and (b) (light blue) correspond to the measurement ranges of Fig. 2.

hybridization of the electronic orbitals due to perturber-induced coupling.

To describe the interaction of a Rydberg atom with a ground-state atom in an external homogeneous electric and magnetic fields, we write down the Hamiltonian,

$$H_{\text{tot}} = H_0 + H_B + H_{\mathcal{E}} + \frac{\mathbf{P}^2}{M} + V_s(\mathbf{r}, \mathbf{R}), \qquad (1)$$

where $\mathbf{P}^2/M$ represents the kinetic energy of the ground-state perturber in a center-of-mass frame, where M is the reduced mass, H_0 is a field-free electron Hamiltonian, and H_B and $H_{\mathcal{E}}$ account for the interaction with the magnetic and electric fields, respectively. In this approach, the total three-body system is described by two relative positions of the ground-state atom $\mathbf{R}$ and of the electron $\mathbf{r}$, taken with respect to the Rydberg ionic core as well as the respective momenta $\mathbf{P}$ and $\mathbf{p}$. Additionally, particles are treated as pointlike. The pseudopotential $V_s(\mathbf{r}, \mathbf{R})$ describing the interaction between the low-energy electron and the perturbing atom takes, in the s-wave regime, the form [14]

$$V_s(\mathbf{r}, \mathbf{R}) = \frac{2\pi\hbar^2 a_s}{m_e}\delta(\mathbf{r} - \mathbf{R}), \qquad (2)$$

where a_s is the s-wave scattering length and m_e is the electron mass. For ^{87}Rb, the triplet scattering length is negative and as a consequence the potential (2) is attractive. Taking into account the local electron density, the resulting potential is proportional to $|\Psi(\mathbf{R})|^2$ [9]. Its modification due to the p-wave shape resonance can result in a binding by internal quantum reflection [15] and in the creation of butterfly-type molecules [16]. Momentum-dependent corrections to the scattering length can be calculated using a semiclassical approximation [17]. We apply a Born-Oppenheimer approximation and express the total wave function as $\Psi(\mathbf{r}, \mathbf{R}) = \psi(\mathbf{r}, \mathbf{R})\phi(\mathbf{R})$, where $\psi(\mathbf{r}, \mathbf{R})$ is the electronic molecular wave function in the presence of the perturber and $\phi(\mathbf{R})$ describes the molecular rovibrational state. This allows for computing the adiabatic potential energy surfaces (APES) for the fine-structure states. Subsequently, one can calculate the molecular binding energies and the rovibrational molecular wave functions by solving the Schrödinger equation using the previously calculated APES. This method was used before for theoretical studies of molecules in external magnetic and electric fields [18–20] and was experimentally verified in Ref. [4].

Here, we are interested in the mixing of two orbitals, $m_j = 5/2$ and $m_j = 1/2$, because of the presence of the neutral atom inside the Rydberg electron orbit, which manifests itself in a change of the molecular binding energy E_B. For fixed electric and magnetic fields, the binding energy E_B of a molecule in a certain configuration is given with respect to the dissociation energy. We treat the molecular potential $V_s(\mathbf{r}, \mathbf{R})$ as a perturbation in first order to the Hamiltonian $H' = H_0 + H_B + H_{\mathcal{E}}$. For the calculation of the full Hamiltonian, we use the basis of $42D_{5/2}$, $m_j = 5/2$ and $42D_{5/2}$, $m_j = 1/2$ electron wave functions,

$$\psi_{1/2}(\mathbf{r}) = R_{42D}(\mathbf{r})Y_{1/2}(\Theta) = \sqrt{\frac{3}{5}}R_{42D}(\mathbf{r})Y_2^0(\Theta)$$
$$\psi_{5/2}(\mathbf{r}) = R_{42D}(\mathbf{r})Y_{5/2}(\Theta, \phi) = R_{42D}(\mathbf{r})Y_2^2(\Theta, \phi), \qquad (3)$$

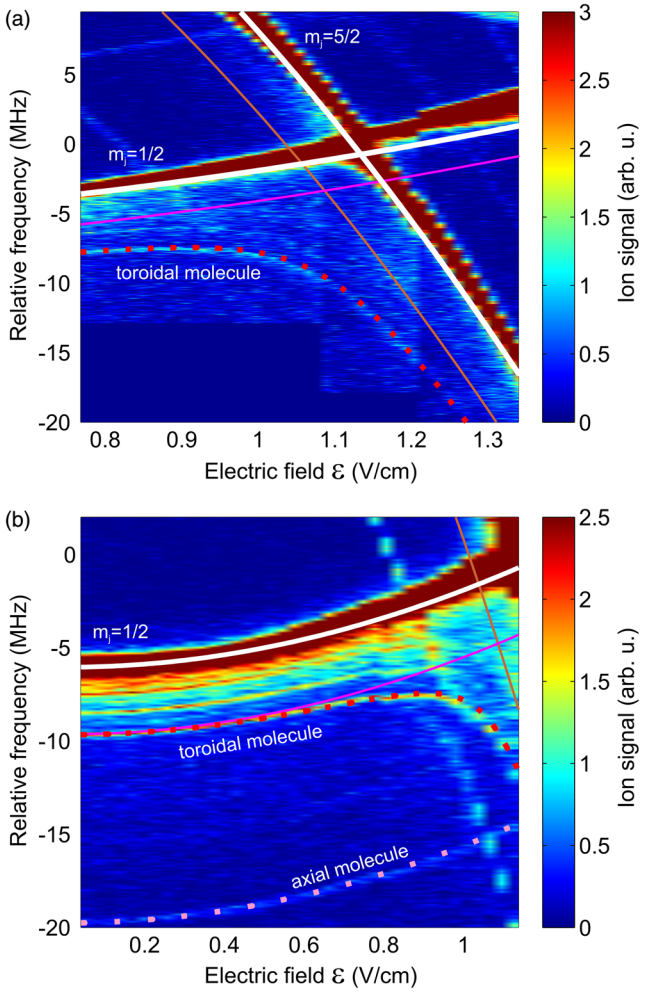

FIG. 2 (color online). Stark map in the vicinity of (a) the degeneracy of the two atomic lines $m_j = 5/2$ and $m_j = 1/2$ and (b) the $m_j = 1/2$ state followed from the zero electric field up to the crossing. Computed atomic-state positions, shown before in Fig. 1, are depicted with continuous white lines. All theoretical molecular lines are plotted with respect to these atomic energy levels. The hypothetical positions of the ground-state toroidal molecular states, with no hybridization of the electron orbital, are indicated with brown and magenta lines, for $m_j = 5/2$ and $m_j = 1/2$, respectively. The binding energy of the toroidal molecule belonging to the $m_j = 1/2$ state changes in the vicinity of the atomic crossing. Calculated positions of the ground-state toroidal and axial molecules are indicated, for the sake of visibility, with red and pink dotted lines, respectively. In addition, excited rovibrational toroidal states are visible in (b). However, it is not possible to accurately trace them for higher electric fields. We identify the weak diagonal lines visible at the higher electric field as laser sidebands with no physical meaning. Note that the atomic lines are saturated due to the chosen color scale. The discontinuity in the $m_j = 1/2$ atomic line above 1.2 V/cm is an experimental artifact.

where we include the respective Clebsch-Gordan coefficients and the spherical harmonics (shown in Fig. 2) in accordance with the triplet state of the electron involved. The radial wave functions are the same for both states. Since we take the unperturbed wave functions as a basis, there is no dependence on $\mathbf{R}$ left. Consequently, we obtain the full Hamiltonian,

$$H = \eta \begin{pmatrix} |Y_{1/2}|^2 + \Delta_1/\eta & Y_{1/2}^* Y_{5/2} \\ Y_{1/2} Y_{5/2}^* & |Y_{5/2}|^2 + \Delta_2/\eta \end{pmatrix}, \quad (4)$$

where $\eta = \eta(\mathbf{R}) = \int d\mathbf{r} V_s(\mathbf{r}, \mathbf{R}) |R_{42D}(\mathbf{r})|^2$ and Δ_1 and Δ_2 are the summed-up energy shifts arising from H'. By diagonalizing the Hamiltonian (4), we obtain the new eigenenergies of the system. The degeneracy between the basis states occurs for $\Delta_1 = \Delta_2$. In the experiment, we can control the energy difference $\Delta = \Delta_2 - \Delta_1$ and thus the mixing of the states by tuning the electric field.

We excite Rydberg atoms in a two-photon process from a magnetically trapped spin-polarized ultracold cloud of ^{87}Rb atoms in the $5S_{1/2}, F = 2, m_F = 2$ state [21] with an applied magnetic offset field of $B = 13.55$ G. The typical temperature of the cloud is 2 μK and the peak density is on the order of 10^{12} cm^{-3}. The 780 nm laser drives the lower transition. The detuning from the intermediate $5P_{3/2}$ state is 500 MHz. The 480 nm laser driving the upper transition is on constantly. After each 50 μs-long 780 nm laser pulse, we ionize Rydberg atoms and molecules with an electric field and detect the ions on a microchannel plate detector. We perform 800 cycles of excitation, ionization, and detection in one cloud while scanning the frequency of the red laser. This way, we obtain one full spectrum of the Rydberg signal for a given value of the electric field. We adjust the polarization of the light driving the upper transition such that the intensities of the two atomic lines close to the crossing (Fig. 1) are comparable.

In Fig. 2, we show the measured Stark maps in the vicinity of the $m_j = 5/2$ and $m_j = 1/2$ atomic states' crossing, marked in Fig. 1 by the green circle. Due to stray electric fields present in the experiment, the electric and magnetic fields are not perfectly parallel. The angle between $\vec{\mathcal{E}}$ and $\vec{B}$ is on the order of a few degrees, which in principle results in a very small coupling between the two atomic states. Nevertheless, given the resolution of our experiment, the considered atomic states appear as a true crossing. The molecular states occur on the red side of the atomic line. The energy difference between the atomic and the molecular peak corresponds to the molecular binding energy E_B. Therefore, we can identify the molecular states by comparing their binding energies at $\mathcal{E} = 0$ with the calculated values [4] by tracing them back to the zero electric field [Fig. 2(b)]. The molecular state visible in the Fig. 2(a) originates from a ground-state toroidal molecule bound in the equatorial plane ($\Theta = \pi/2$) of the $m_j = 1/2$ scattering potential (see inset of Fig. 1) with $E_B =$ 3.6 MHz at $\mathcal{E} = 0$. The molecular ground-state bound in the axial lobe ($\Theta = \pi, 0$) of the same scattering potential occurs at $E_B = 13.7$ MHz for $\mathcal{E} = 0$. While changing the

electric field, this axial molecule follows in parallel the trace of the $m_j = 1/2$ atomic line up to the degeneracy point, whereas the toroidal bends around the crossing and asymptotically follows the $m_j = 5/2$ atomic line. In the experiment, we are able to address the individual rovibrational molecular states visible in the Fig. 2(b). However, since the excited toroidal states are blurred near atomic degeneracy, we focus our analysis on the molecular ground states.

Assuming no hybridization, the molecular states of the $m_j = 1/2$ and $m_j = 5/2$ would occur at a constant binding energy $E_B(\mathcal{E} = 0)$ with respect to the corresponding atomic lines regardless of the applied electric field. In Fig. 2, such unperturbed ground-state toroidal molecule traces, plotted in reference to the calculated atomic energy levels, are shown for the $m_j = 1/2$ and $m_j = 5/2$ states with continuous brown and magenta lines, respectively. These two states, described by the wave functions (3), form a basis for our two-level model. Consequently to predict the behavior of the perturbed hybrid states, we calculate the eigenenergies $E_\pm$ of the Hamiltonian (4). For a given molecular state, the obtained analytical solution depends only on the energy difference Δ between the $m_j = 1/2$ and $m_j = 5/2$ states and a parameter η, which is determined from the fitting of E_+ to the experimental data at $\mathcal{E} = 0$. In the experiment, the energy difference Δ around the crossing depends to a good approximation linearly on the electric field. E_-, which would correspond to the toroidal molecule of the $m_j = 5/2$ state, was not observed in this experiment. By calculating E_+, i.e., the predicted binding energy, as a function of $\Delta(\mathcal{E})$, we reproduce the behavior of the toroidal and axial molecular lines (Fig. 2) with high accuracy. Note that the modeled molecular traces are plotted with respect to the computed atomic positions. The scattering potential couples the unperturbed toroidal molecular lines, although the respective atomic states cross without any level repulsion between them. This leads to orbital mixing and therefore a change in the Rydberg electron probability density, which we observe as an increased binding energy of the toroidal molecule. In the case of the axial molecule, the of-diagonal coupling terms in the Hamiltonian (4) vanish. This is due to the fact that the toruslike $m_j = 5/2$ spherical harmonic is zero along the axial direction and thus does not modify the $m_j = 1/2$ state in this direction. For this reason, the binding energy stays constant.

In Fig. 3, the measured and calculated (E_+) binding energies of the considered molecules versus the electric field are shown. Here, the binding energy is determined as the difference between the measured atomic and molecular energies. The binding energy of the toroidal molecules increases from $E_B(\mathcal{E} = 0)$ of the $m_j = 1/2$ state, reaches its maximum of $E_B = 11.7$ MHz, and asymptotically decreases to $E_B(\mathcal{E} = 0)$ of the $m_j = 5/2$ state. This transition can be attributed to an increase of the admixture of the $m_j = 5/2$ state from 0 to 100%. The maximum

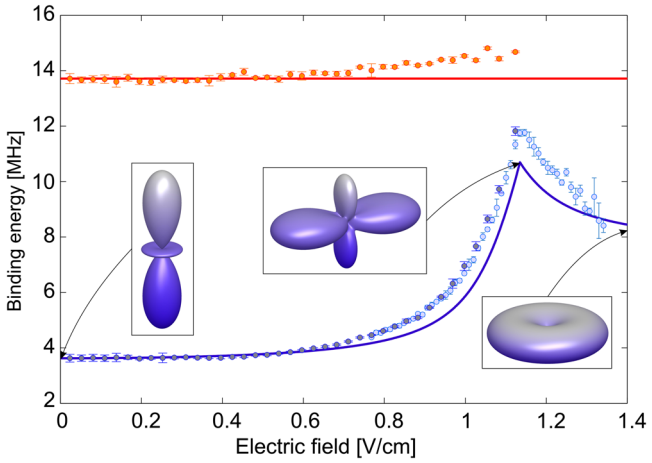

FIG. 3 (color online). Measured binding energies of the axial (orange points) and toroidal ground-state molecules (light blue and violet points) versus the electric field. The binding energies are extracted from two data sets shown in Figs. 2(a) and 2(b) and hence indicated with two colors for the toroidal molecule data. A ground-state atom inside the Rydberg electron in the toroidal plane mixes two orbitals. As a result, the binding energy of the $m_j = 1/2$ toroidal molecule increases, reaches its maximum directly at the crossing, and then asymptotically decreases to the E_B value of the $m_j = 5/2$ toroidal molecule. Shown in the inset is the relevant part for molecule formation of the spherical harmonic of the hybridized Rydberg orbital at the crossing, together with the two asymptotic shapes. The error bars are determined as 2 standard deviations of the fit.

binding energy corresponds to an orbital consisting of 50% $m_j = 1/2$ character and 50% $m_j = 5/2$ character. The resulting shape of the orbital is shown in the inset of Fig. 3. The hybridization introduces a ϕ dependence to the Rydberg orbital, even though the asymptotic states were spherically symmetric along the z axis. For the unperturbed axial molecule, the shape of the Rydberg orbital remains the same.

Directly at the crossing, the experimental binding energy of the toroidal molecule and the calculated one deviate by 9%. The predominant reason for the discrepancy around the crossing, for $\mathcal{E} > 0.8$ V/cm, is the difficulty in determining the atomic peak position caused by the non-Gaussian shape of the peak. Additionally, for $\mathcal{E} > 1.2$ V/cm, fitting of the molecular state position becomes problematic. Moreover, for the calculation, we only take into account the unperturbed states and not the real Stark states. Finally, more levels could be included into the analysis. In view of these facts, the agreement between the experimental data and our simple model is remarkable. A more complicated analysis would not lead to a significantly better agreement resulting from the purely experimental constraints.

We have shown the hybridization of the Rydberg electron orbital due to the molecule formation around the crossing of the atomic lines $m_j = 1/2$ and $m_j = 5/2$. The backaction of the bound perturber increases

the binding energy and consequently changes the shape of the electron orbital. Mixing more than two electron orbitals of known shapes by bringing them to degeneracy could result in even more complex asymmetric electron configurations. Furthermore, the influence of a different type of perturber, like an atom of another element or a heteronuclear molecule [22], as well as the effect of a few perturbers on the electron orbital could be investigated. A Rydberg electron orbital hybridized due to thousands of the ground-state perturbers could be observed as an imprint on a Bose-Einstein condensate [23]. Finally, engineering a state by placing the perturber precisely at a desired position might also be feasible in experiments with individual atoms in microtraps.

We acknowledge support from the Deutsche Forschungsgemeinschaft (DFG) within the SFB/TRR21 and Project No. PF 381/13-1. Parts of this work were also funded by the ERC under Contract No. 267100. A. G. acknowledges support from the E. U. Marie Curie program ITN-Coherence 265031 and S. H. from DFG through the Project No. HO 4787/1-1.

A. G. and A. T. K. contributed equally to this work.

*a.gaj@physik.uni-stuttgart.de
†t.pfau@physik.uni-stuttgart.de

[1] L. Pauling, J. Am. Chem. Soc. **53**, 1367 (1931).
[2] V. Bendkowsky, B. Butscher, J. Nipper, J. P. Shaffer, R. Löw, and T. Pfau, Nature (London) **458**, 1005 (2009).
[3] J. Tallant, S. T. Rittenhouse, D. Booth, H. R. Sadeghpour, and J. P. Shaffer, Phys. Rev. Lett. **109**, 173202 (2012).
[4] A. T. Krupp, A. Gaj, J. B. Balewski, P. Ilzhöfer, S. Hofferberth, R. Löw, T. Pfau, M. Kurz, and P. Schmelcher, Phys. Rev. Lett. **112**, 143008 (2014).
[5] D. A. Anderson, S. A. Miller, and G. Raithel, Phys. Rev. Lett. **112**, 163201 (2014).
[6] M. A. Bellos, R. Carollo, J. Banerjee, E. E. Eyler, P. L. Gould, and W. C. Stwalley, Phys. Rev. Lett. **111**, 053001 (2013).
[7] H. Saßmanmhausen, F. Merkt, and J. Deiglmayer, Phys. Rev. Lett. **114**, 133201 (2015).
[8] A. Gaj, A. T. Krupp, J. B. Balewski, R. Löw, S. Hofferberth, and T. Pfau, Nat. Commun. **5** (2014).
[9] C. H. Greene, A. S. Dickinson, and H. R. Sadeghpour, Phys. Rev. Lett. **85**, 2458 (2000).
[10] D. Booth, S. Rittenhouse, J. Yang, H. Sadeghpour, and J. Shaffer, Science **348**, 99 (2015).
[11] W. Li *et al.*, Science **334**, 1110 (2011).
[12] W. Li, I. Mourachko, M. W. Noel, and T. F. Gallagher, Phys. Rev. A **67**, 052502 (2003).
[13] M. Mack, F. Karlewski, H. Hattermann, S. Höckh, F. Jessen, D. Cano, and J. Fortagh, Phys. Rev. A **83**, 052515 (2011).
[14] E. Fermi, Nuovo Cimento A **11**, 157 (1934).
[15] V. Bendkowsky *et al.*, Phys. Rev. Lett. **105**, 163201 (2010).
[16] E. L. Hamilton, C. H. Greene, and H. R. Sadeghpour, J. Phys. B **35**, L199 (2002).
[17] A. Omont, J. Phys. (Orsay, Fr.) **38**, 1343 (1977).
[18] I. Lesanovsky, P. Schmelcher, and H. R. Sadeghpour, J. Phys. B **39**, L69 (2006).
[19] M. Kurz and P. Schmelcher, Phys. Rev. A **88**, 022501 (2013).
[20] M. Kurz and P. Schmelcher, J. Phys. B **47**, 165101 (2014).
[21] R. Löw, H. Weimer, J. Nipper, J. B. Balewski, B. Butscher, H. P. Büchler, and T. Pfau, J. Phys. B **45**, 113001 (2012).
[22] R. González-Férez, H. R. Sadeghpour, and P. Schmelcher, New J. Phys. **17**, 013021 (2014).
[23] T. Karpiuk, M. Brewczyk, K. Rzażewski, A. Gaj, J. B. Balewski, A. T. Krupp, R. Löw, S. Hoffereberth, and T. Pfau, New J. Phys. **17**, 053046 (2015).